energies

MDPI

Article

A Class-E Amplifier for a Loosely Coupled Inductive Power Transfer System with Multiple Receivers

Alexander Sutor [1,*], Martin Heining [2] and Rainer Buchholz [2]

1. Institute of Measurement and Sensor Technology, UMIT—Private University for Health Sciences, Medical Informatics and Technology GmbH, Eduard-Wallnöfer-Zentrum 1, 6060 Hall in Tirol, Austria
2. Institute of Bioprocess Engineering, Friedrich-Alexander-University Erlangen-Nuremberg, Paul-Gordan-Straße 3, 91052 Erlangen, Germany; martin.heining@bvt.cbi.uni-erlangen.de (M.H.); Rainer.Buchholz@bvt.cbi.uni-erlangen.de (R.B.)

* Correspondence: alexander.sutor@umit.at; Tel.: +43-50-8648-3885

Received: 1 March 2019; Accepted: 20 March 2019; Published: 26 March 2019

check for updates

Abstract: We present a method for optimizing the electronic power system for a new type of photobioreactor or photoreactor in general. In the case of photobioreactors, photosynthetic active microorganisms or cells are grown. A novel concept for the illumination of photobioreactors was necessary, as the external illumination of those reactors leads to a limited penetration depth of light. Due to the limited penetration depth, no standard reactors can be use for cultivation, but custom made reactors with very small volume to surface ratio have to be used. This still prevents the technology from a large scale industrial impact. The solution we propose in this paper is an internal illumination via Wireless Light Emitters. This increases the manageable culture volume of photosynthetic active microorganisms or cells. The illumination system is based on floating light emitters, which are powered wirelessly by near field resonant inductive coupling. The floating light emitters are able to illuminate a photobioreactor more homogeneously than external illumination systems do. We designed a class-E amplifier and field coils to produce an intermediate frequency electromagnetic field inside the reactor. An appropriate magnetic flux density was found to be approx. $B = 1\,\mathrm{mT}$ and the driving frequency is $f = 176\,\mathrm{kHz}$. We conducted experiments with a laboratory size photoreactor. The cultivation volume was 30 L containing up to 3000 WLEs. The maximum electric power input was more than 300 W and we calculated an efficiency of up to 76%.

Keywords: wireless power transfer; photobioreactor; wireless light emitter; class-E amplifier

1. Introduction

Wireless power transfer is a classic engineering field currently gaining increasing attention. One reason is the wide variety of applications. It ranges from consumer products like electric tooth brushes and charging of mobile phones to high end medical applications [1–5] like cochlear implants [6], wireless endoscopic capsules [7,8], and cardiac pacemakers [9]. Recently, some effort has been put into the development of contactless charging systems for electric vehicles. The authors of [10] presented a loosely coupled transformer system for charging an electric vehicle with up to 4 kW power. They used a full-bridge inverter on the primary side and realized zero-voltage switching (ZVS). Ville at al. give the perspective up to a charging power of 200 kW for a similar system [11]. The advantages of ZVS have also been proven for a high frequency single phase inverter [12]. Another transformerless ZVS full-bridge inverter was shown to be more efficient compared to commercial H6 inverters [13].

The class-D amplifier is the most popular topology in wireless power applications. In principle, the class-E amplifier is superior in terms of efficiency and was originally published by Sokal [14]. The reason for its efficiency is that it allows not only ZVS but also zero-derivative switching (ZDS) [15].

This fact further reduces switching losses. In a few areas the class-E amplifier is applied already. High frequency application reaches into the megahertz and microwave range [16,17], while most applications are found in the intermediate frequency electromagnetic field (IF-EMF) range. Highly efficient class-E power amplifiers are typically used in cochlear implants [6]. Its application for a Bone Conduction Implant has been published by Taghavi et al. [18]. Wang et al. use a class-E amplifier for wirelessly powering a retinal prosthesis [19]. Recently, suggestions for the use of class-E amplifiers in high power applications like the charging of electric vehicles have also been published [20].

We have already published the principle idea behind internal illumination by Wireless Light Emitters (WLE) and presented preliminary results for the application in photobioreactors [21] as well as photocatalytical reactors [22]. We have also reported on promising results for algae cultivation by WLE before [21,23] and compared our system other developments [24]. In this paper, we discuss the use of a class-E amplifier for efficiently powering internally illuminated photobioreactors. We present methods for designing and optimizing the amplifier with respect to the boundary conditions given by a desired photobioreactor (PBR) setup. We discuss the source of losses and methods for their minimization.

The paper is structured as follows. In Section 2, the internal illumination is motivated and our test systems are described. We explain why the class-E amplifier is especially suitable to power a loosely coupled system in Section 3 and present a SPICE model for the simulation of an arbitrary number of receivers or WLEs. Section 4 explains how the network elements are chosen appropriately. Simulation as well as measurement results are presented in Section 5. Those results are discussed in Section 6. Conclusions are drawn in Section 7 and possible improvements are motivated.

2. Internal Illumination of Photobioreactors

The dominant growth affecting parameter for photoautotrophic microalgae cultures is light, which is absorbed by the microalgae and drives photosynthesis. This absorption leads to an exponential attenuation of the light intensity for increasing culture depths and cell densities according to Lambert-Beer's law of extinction. This fact limits the photobioreactors to small diameter systems and hinders the development of industrial relevant scale ups. An overview on the light requirements in microalgal photobioreactors is, for example, given by Carvalho et al. [25].

The idea of internally illuminated photobioreactors has come up in the 1990s and various systems have been developed since. Recently, the interest in these systems has been on the rise again, due to the increased production of and research on high-value products and recombinant proteins from microalgae and plant cell cultures. While promising results in lab-scale have been achieved, the potential of photoautotrophic or mixotrophic production of these compounds is limited due to the lack of scalable photobioreactors, which could be overcome by internally illuminated systems.

2.1. Earlier Approaches

An elaborate review on recent approaches is given in [24]. Here, we only want to provide a short overview. Internally illuminated PBRs (IIPBR) can in principle be divided into two major categories: reactors which transport the light into the inside by light guides and reactors actually containing internal light sources. The reactors of the first type are characterized by some sort of light-collecting device outside the reactor and a light guide to transport the light to a radiator within the culture volume. Those kinds of IIPBRs can further be subdivided by the nature of the light-distributing device. It can either consist of optical fibers, optical plates or some other kind of structure. The second class is characterized by actually having a light source inside the reactor. There are different ways to classify these kinds of IIPBRs, for example by the type of light source being used (e.g., fluorescent lamps, metal halide lamps or LEDs). A further classification discriminates between static, built-in light sources and dynamic, mobile light sources. The latter is the most promising approach and has been the motivation for the development of WLEs.

2.2. Internal Illumination via WLEs

2.2.1. Construction of the WLE

The circuit of the WLE is a parallel connection of a receiving coil, a capacitor and a LED. The LED is a warm white Cree® CLM3A in a PLCC2 package with an operating point $V_F = 3.2\,\mathrm{V}$, $I_F = 20\,\mathrm{mA}$. The peak forward current is $I_{FP} = 100\,\mathrm{mA}$. Its color temperature is 3200 K and the typ. luminous flux is 3.9 lm. The coils are SMD SDR0403-100ML power inductors from Bourns®. The inductance is $L = 10\,\mu\mathrm{H}$ and the series resistance is $R_{DC} = 0.18\,\Omega$. The value of the capacitance is $C = 82\,\mathrm{nF}$. This results in an eigenfrequency

$$f = \frac{1}{2\pi\sqrt{LC}} \quad \text{or} \quad f = \frac{1}{2\pi}\sqrt{\frac{1}{LC} - \frac{R_L^2}{L^2}} \tag{1}$$

depending on whether to take the series resistance into account. For the undamped circuit we get $f = 176\,\mathrm{kHz}$. The small series resistance has practically no influence on the resonance frequency, but has to be taken into account when dealing with loss aspects. The circuit has been encapsulated into an ethylene propylene diene monomer sphere, see Figure 1.

The typical density of WLE distribution in our reactors is 125 WLEs per liter which results in an average pickup power density of 10 W/L. In an earlier publication, we have already presented measurements that show that for diameters larger than 5 cm, internal illumination is far more homogeneous than external illumination [21].

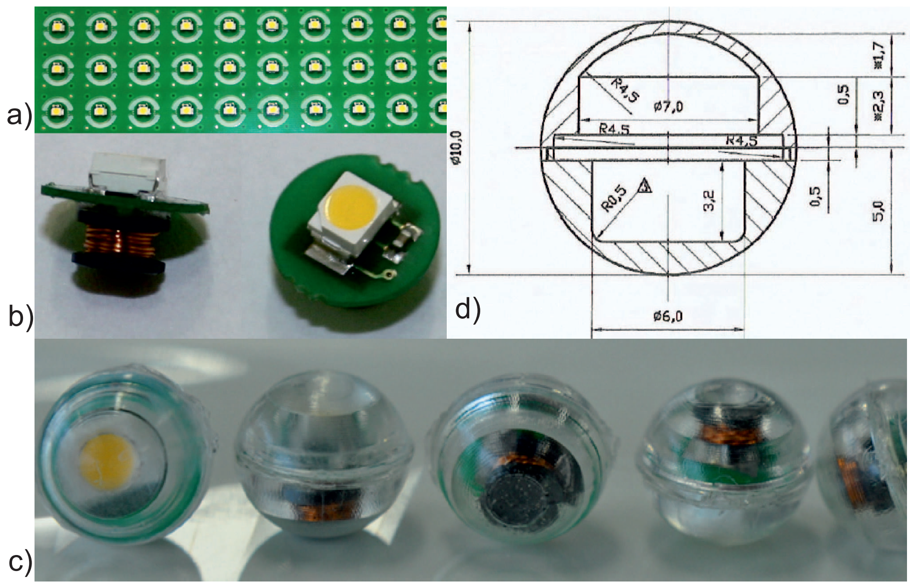

Figure 1. (**a**) series production on professional PCB board; (**b**) close-up of side view and top view; (**c**) encapsulated Wireless Light Emitters (WLE); (**d**) construction drawing.

2.2.2. Reactor and Driving Coils

Our demonstrator setup consists of an airlift reactor fabricated from glass. Its diameter is 300 mm and its height is 350 mm. In operation the reactor contains a maximum of 3000 WLEs, see Figure 2c. The reactor is equipped with four driving coils consisting of 30 windings each.

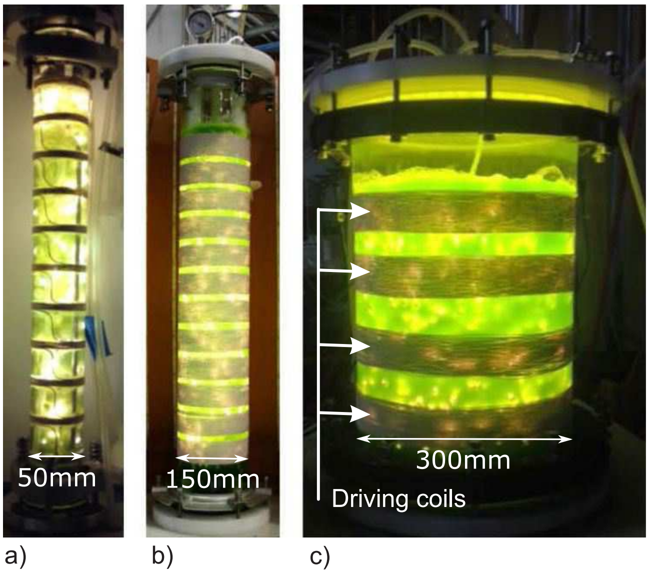

Figure 2. Three test reactors with diameters of (**a**) 50 mm, (**b**) 150 mm, and (**c**) 300 mm. The largest reactor with the four tagged driving coils has been used in the experiments described here.

The four coils are connected in parallel which gives a total inductance of $L = 338\,\mu\text{H}$. Due to the relatively high frequency, Litz wire has to be used to reduce the skin effect. The penetration depth δ due to the skin effect can be calculated by

$$\delta = \frac{1}{\sqrt{\pi f \lambda \mu}}\,, \tag{2}$$

where λ is the electric conductivity and µ is the permeability of the medium. For copper wire, which has an electric conductivity of $\lambda = 56\,\text{MS/m}$, the penetration depth is 160 µm. Therefore, we use RUPALIT V155 consisting of 80 strands with a diameter of 100 µm each.

It must also be mentioned that eddy currents in saline water also have to be taken into account for larger diameters of the reactor. A medium which contains 3 g/L NaCl, as used for cultivating the green alga *Chlamydomonas reinhardtii*, leads to an electric conductivity of the medium of $\lambda = 0.5\,\text{S/m}$. This results in a penetration depth of 1.69 m according to Equation (2). It is even more important to look at the eddy current losses. According to Fiorillo [26], the eddy current loss density p in W/m^3 for sinusoidal fields can be calculated by

$$p = \frac{\pi^2}{3}\lambda B^2 f^2 r^2\,. \tag{3}$$

For the given geometry and medium, this results in a loss density $p = 1690\,\text{W/m}^3$ and a total loss of 50.7 W in the 30 L volume reactor (Figure 2c) with an assumed magnetic flux density $B = 1\,\text{mT}$ and a radius $r = 150\,\text{mm}$.

3. The Principle of Loose Coupling with Multiple Receivers

A problem when dealing with multiple receivers occurs from the fact that the orientations of sending and receiving coils are not necessarily in parallel. There are several ways to solve this issue. The direction of the magnetic field vector could be rotated in space for example by using several sending coils [27]. In addition, a set of three receiving coils is possible, a solution which consumes additional space in the receiver [7]. We solved the problem by setting the center of mass in the lower part of the WLE, so that it is oriented automatically in the air lift.

3.1. Simulations on Topology Issues

In literature there is some discussion going on about the topology of primary and secondary circuit. Topology in this context refers to serial or parallel connection of the resonant elements. The authors of [28] claim that serial connection on the secondary side is superior to parallel connection. We want to show in the following that this depends on the magnitude of the impedances of the used network elements. Kuipers et al. [29] use a serial receiving circuit to drive a UV-LED from Nichia, type NSPU510CS. The allowed forward current is in the range of 20 to 80 mA at a typical voltage of 3.3 V. They use a $L = 10$ mH receiving inductance with a quality factor of 90 at their working frequency 45 kHz and parasitic series resistance of $R_L = 1.26\ \Omega$ and a 1 nF capacitor. The sending inductance is $L = 1.4$ mH and the coupling factor is $k = 0.02$. The circuit for the described setup is depicted in Figure 3.

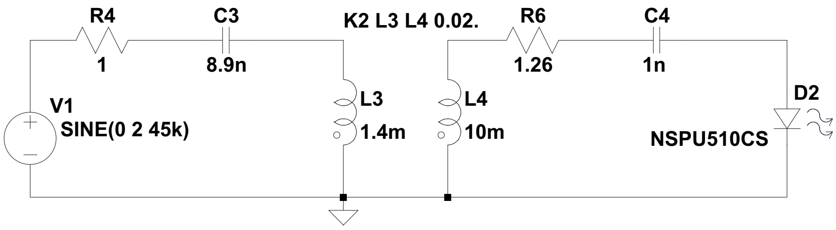

Figure 3. Lumped network of the receiver in parallel connection as proposed in [29].

A simple simulation reveals that the circuit in this form will not work as the resistance of the LED in reverse direction is too high.

There are two possibilities to improve the circuit. Firstly, a much larger capacitance can be chosen which will result in a non-resonant circuit. Due to the very large inductance of $L = 10$ mH, a peak current of 15 mA can be reached for an arbitrary capacitance value of 1 mF. In order to utilize the resonant properties with the original 1 nF capacitance, a series circuit as depicted in Figure 4 has to be chosen for the right hand side. In this case, the simulation leads to a similar peak current of 16 mA. A further increase of the peak current can be achieved if the impedances of the inductance and the capacitance are decreased. A pairing of $L = 1$ mH and $C = 10$ nF will increase the peak current to over 50 mA.

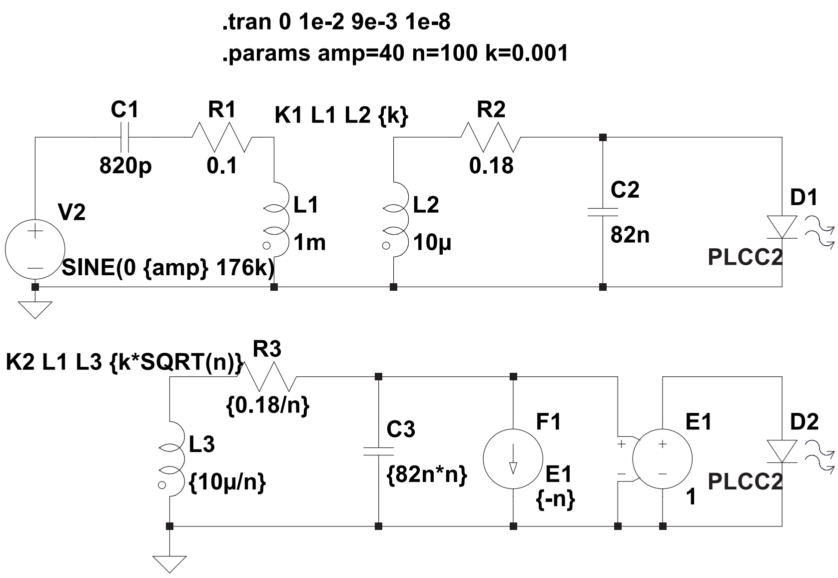

Figure 4. The upper righthand circuit represents a single WLE-receiver. The lower circuit stands for a lumped network of n receivers.

It can be concluded that a parallel resonant circuit has to be chosen for the receiving side and that the impedances of L and C significantly influence the peak current.

3.2. Simulations on Multiple Receivers

As we have up to 3000 receivers, the simulation of single receivers is not possible. Therefore, we want to find equivalent circuits for the receivers. Without loss of generality, we can draw all receivers to the same ground. Since the receivers are identical, we can assume the upper potential to be the same and we get a parallel connection of all receiver elements. The only restriction is that the coupling factor has to be equal for all receivers. This fact certainly does not model reality perfectly, but the coupling factor for a single receiver is hardly possible to determine anyways.

The equivalent network is given in Figure 4. The parameter n stands for the number of WLEs. The LEDs are models with part NSSW008CT-P1 from the LTSpice library, whose parameters are very similar to the characteristics in the Cree® CLM3A datasheet.

The equivalent network elements are derived as follows. Let us assume a transformer with one primary inductance L_1 (sending coil) and n secondary inductances L_2 (the WLEs). The secondary inductances do not couple among each other, but each has the mutual inductance M with the primary side. This transformer can then be described by

$$\begin{aligned} U_1 &= \mathrm{j}\omega L_1 I_1 + n \cdot \mathrm{j}\omega M I_2; \\ U_2 &= \mathrm{j}\omega M I_1 + \mathrm{j}\omega L_2 I_2, \end{aligned} \tag{4}$$

where U_1 and U_2 are voltages and I_1 and I_2 are the currents on the primary and secondary side, respectively. If we draw all receivers to the same ground and if we can further assume that the upper potentials are equal, as motivated above, we can substitute the n right-hand sides by an equivalent inductance $L_{2,eq}$, which is flown through by the equivalent current $I_{2,eq}$ and which incorporates the mutual inductance M_{eq} with the left-hand side. This equivalent transformer is described by the equations

$$\begin{aligned} U_1 &= \mathrm{j}\omega L_1 I_1 + \mathrm{j}\omega M_{eq} I_{2,eq}; \\ U_2 &= \mathrm{j}\omega M_{eq} I_1 + \mathrm{j}\omega L_{2,eq} I_{2,eq}. \end{aligned} \tag{5}$$

By comparing Equations (4) and (5), one can express the equivalent network elements and values by the original ones

$$\begin{aligned} M_{eq} &= M; \\ I_{2,eq} &= n \cdot I_2; \\ L_{2,eq} &= L_2/n. \end{aligned} \tag{6}$$

The coupling factor between the sending coil and each receiver is defined by

$$k = \frac{M}{\sqrt{L_1 L_2}}. \tag{7}$$

Using the equivalent elements from Equations (6), the equivalent coupling factor can be written as

$$k_{eq} = \frac{M_{eq}}{\sqrt{L_1 L_{2,eq}}} = \frac{M}{\sqrt{L_1 L_2/n}} = \sqrt{n}k. \tag{8}$$

Furthermore, the parasitic series resistances of all receiver coils R_L are virtually put in parallel, so are the receivers' capacitances C. This results in equivalent elements

$$R_{L,eq} = R_L/n \quad \text{and} \quad C_{eq} = nC. \tag{9}$$

The fact that n LEDs have to be put in parallel is modeled by the current controlled current source $F1$, see Figure 4, which multiplies the LED current by n. The negative sign follows the current counting direction of the voltage source $E1$. With this method, multiple WLEs can be taken into account simply by setting the parameter n in the SPICE parameter set.

4. Tuning the Class-E Amplifier

The basic circuit for a class-E amplifier is given in Figure 5. In the following, the equations for tuning the amplifier's network elements are only briefly given, as the method and derivation of the equations have been described elsewhere [30]. A duty cycle of 50% shall be fixed. The frequency f, inductance of transmitting coil L and required power P_0 in the load are given.

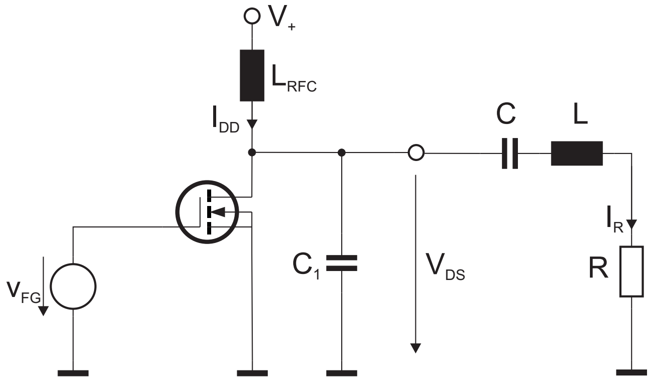

Figure 5. Most basic circuit for the class-E amplifier.

The load R models and replaces the total active load in Figure 4. It has to be calculated from the active power pick up into L_1 and is only valid for a specified working point, as is the following calculation. Therefore, the amplifier has to be tuned for a given working point. The angular frequency is $\omega = 2\pi f$. The switch is opened at $\omega t = 0$ and closed at $\omega t = \pi$. The switching angle ϕ describes the phase of output current i_R with respect to ωt. An optimal switching angle, which assures ZVS and ZDS, was found to be

$$\phi_{opt} = \arctan \frac{-2}{\pi}. \tag{10}$$

With help of the optimal switching angle, the shunt capacitance C_1 can already be determined

$$C_1 = \frac{-2\sin(2\phi_{opt})}{\pi^2 \omega R}. \tag{11}$$

The capacitance C can be calculated with the following equations, which have been derived in [31]:

$$C = (QR\omega - L_X\omega^2)^{-1}, \tag{12}$$

with

$$L_X = \frac{R}{\omega}\tan(\phi_1 - \phi_{opt}) \tag{13}$$

and

$$\phi_1 = \arctan \frac{\frac{8}{\pi^2} - 1}{\tan \phi_{opt}}. \tag{14}$$

Furthermore, the amplitude of the output current $\hat{i}_R$ can be calculated

$$\hat{i}_R = \sqrt{\frac{2P_0}{R}}. \tag{15}$$

Another important parameter is the quality factor

$$Q = \frac{\omega L}{R}, \tag{16}$$

which has to be high enough to assure sinusoidal current i_R. As a rule of thumb it can be stated that Q shall be at least larger than five. For our reactors, we measured $Q \approx 20$ (see Equations (20) and (21)), which makes the class-E amplifier especially suitable here.

In order to determine the requirements for the power source, the necessary source current I_{DD} and voltage V_+ are calculated by

$$I_{DD} = 2\hat{i}_R \frac{\cos\phi}{\pi} \quad \text{and} \quad V_+ = \frac{P_0}{I_{DD}}. \tag{17}$$

Finally, the choke inductance L_{RFC} can be dimensioned to gain DC current I_{DD} containing low ripple according to [32]

$$L_{RFC} = \frac{(\pi^2 + 4)R}{16 f r_{ss}}, \tag{18}$$

where r_{ss} denotes the allowed relative ripple.

In order to demonstrate the concept, we have constructed two amplifiers with different maximum power P_0. Amplifier #1 is based on the Transistor IRFB4019 from International Rectifier and allows a maximum drain-source voltage of 150 V. We reached a maximum power of 55 W. The amplifier #2 works with a IPW60R045 transistor from Infineon. The maximum drain-source voltage is 600 V and the on-resistance is extremely low at 45 mΩ. With amplifier #2 a maximum power of 300 W was reached.

Figure 6 shows the simulation results for amplifier #1. The figure shows the important time signals. Especially the drain source voltage V_{DS} is important to judge the tuning of the amplifier. The arrows indicate in which way the signal is influenced by increasing capacitances C and C_1. The values for the tuned amplifier are $C = 790.2$ pF and $C_1 = 11.5$ nF. For an intentionally mistuned example, the values have been changed to $C = 785$ pF and $C_1 = 10$ nF.

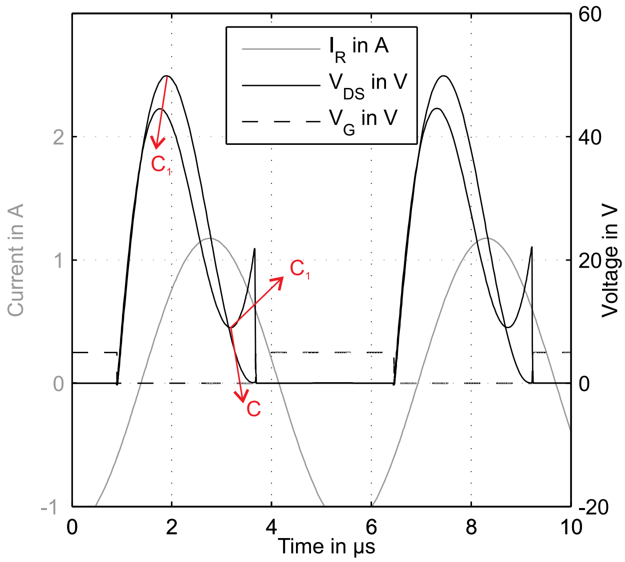

Figure 6. Simulations of a tuned and a mistuned amplifier. The arrows indicate the direction into which the minimum moves when changing the values for C and C_1.

5. Results

Figure 7 shows some measurement results of amplifier #1 for little load which consumes approximately 9 W. The circuit is well tuned. The time signals are very much in accordance to the simulations shown in Figure 6. The amplifier at its maximum power produces the signals in Figure 8. A look at the gate voltage reveals what happens in the case of mistuning: the zero voltage condition is not yet reached at the time the switch is opened, which leads to a voltage jump and subsequent damped oscillation. In the case shown here, the capacitance C_1 is too large.

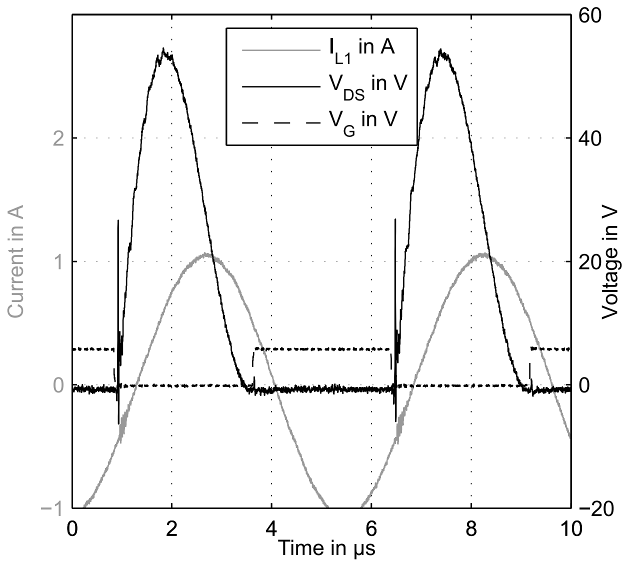

Figure 7. Some measured signals. Notice that the amplifier is well tuned. The output power is approx. 9 W.

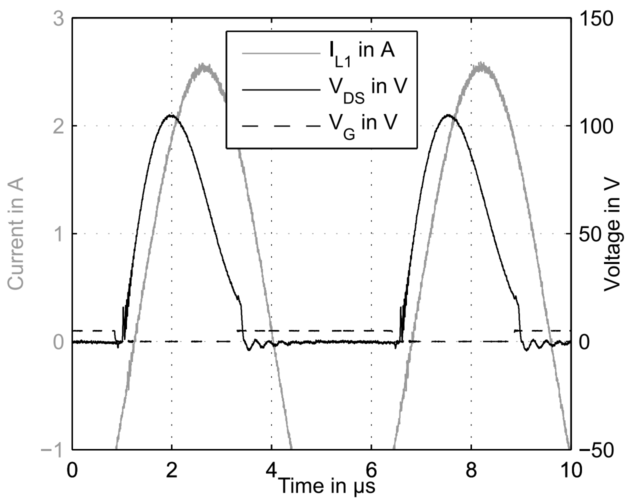

Figure 8. The amplifier is mistuned at its maximum power of 55 W.

5.1. Simulation of the 300 W Amplifier #2 with 3000 WLEs as Load

Figure 9 shows the circuit for the 300 W class-E amplifier #2 including 3000 WLEs as load. The figure also contains dimensions, simulation information and SPICE commands for some calculations on the losses within certain network elements by integrating the power signals. The source produces a power of 250.2 W at a voltage of 140 V. The losses are so small that the sending coil L_1 can deliver active power of 245.1 W. The main losses occur in the series resistance of the receiving coils R_1, which sum up to a total of 47.7 W. The LEDs finally receive 197.4 W.

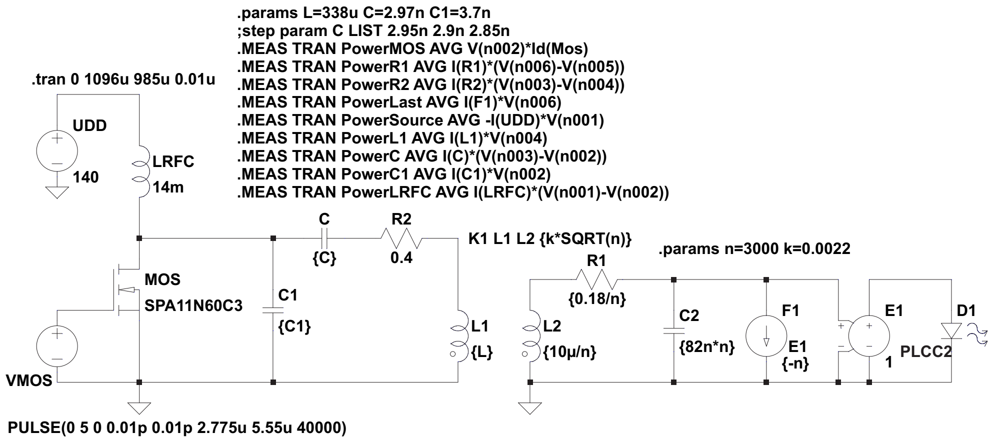

Figure 9. Complete circuit of the 300 W amplifier #2 including a load of 3000 WLEs.

Important simulated signals can be found in Figure 10. The gate voltage V_G shows the switching points. The sending coil current I_{L1} shows quite a sinusoidal trend. Notice the increase of the coil voltage V_{L1} at the point in time when the MOSFET opens. When the MOSFET closes again, the drain-source voltage V_{DS} reaches ZVS and ZDS conditions.

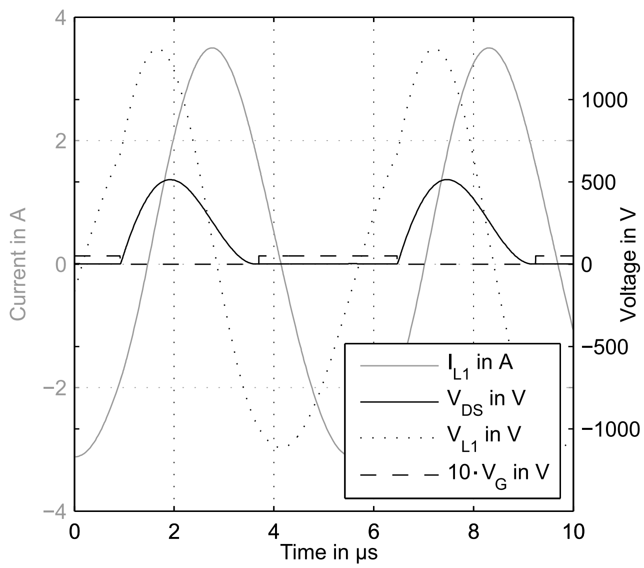

Figure 10. Simulation results for amplifier #2.

5.2. Measurements

According to the principle circuit given in Figure 5, the amplifier #2 was constructed. In order to provide the necessary power at node V^+, two adjustable current sources HVGC-150-1400 from Mean Well were used in parallel. Each provides a constant current up to 1.4 A up to a maximum voltage of 107 V. The measured coil current I_{L1}, the drain-source voltage V_{DS} and the gate voltage V_G are depicted in Figure 11. The current sources deliver a power of approx. 250 W. The measured signals at the max. power of approx. 300 W are shown in Figure 12. Additionally, the current in the choke I_{RFC} is depicted.

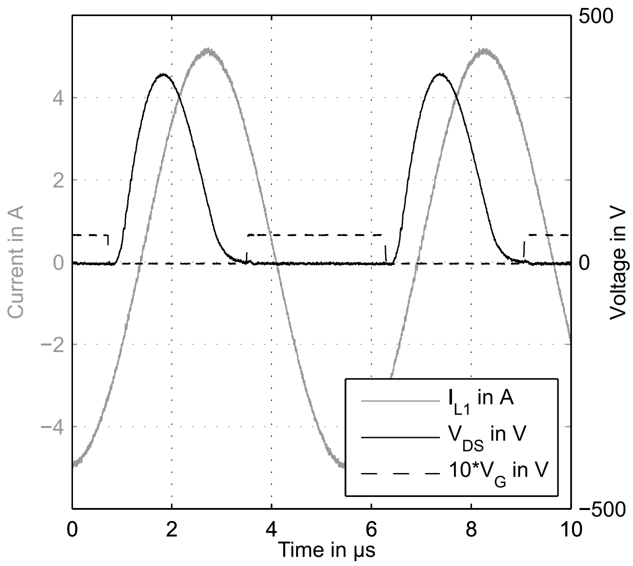

Figure 11. Measurement results for amplifier #2. Active power approx. 250 W.

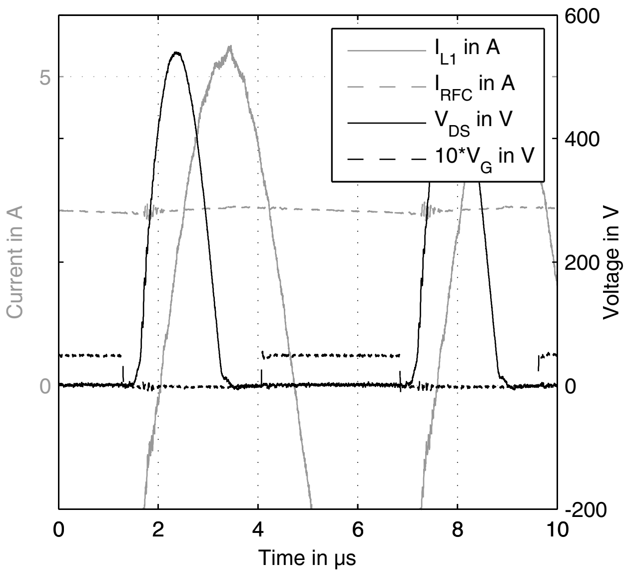

Figure 12. Measurement results for amplifier #2. Active power approx. 300 W.

6. Discussion

In order to judge the quality of the system, two values are calculated. Firstly, in order to characterize the amplifier itself, a pure electrical measure is taken, namely the efficiencies of the electric transformations. Secondly, the efficiency of the biomaterial production is determined by comparing our internally illuminated reactor to external illumination.

The measured power at plug socket (P_{PS}), current source output (P_{CS}), and driving coil input (P_L) are compared in Table 1. The efficiency is calculated for the current source η_{CS} and for the class-E amplifier alone η_E using the relations

$$\eta_{CS} = \frac{P_{CS}}{P_{PS}} \quad \text{and} \quad \eta_E = \frac{P_E}{P_{CS}} \,. \tag{19}$$

Finally, the total efficiency $\eta_t = \eta_{CS} \cdot \eta_E$ is given. The maximum efficiency of the current source is in accordance to the manufacturer's specifications.

Table 1. Active power and efficiency aspects.

P (W)	P_{PS}	P_{CS}	η_{CS}	P_L	η_E	η_t
min.	116	93.6	80.7%	65.2	69.7%	56.2%
	179	157	87.7%	114	72.6%	63.7%
	216	198	91.6%	150	75.7%	69.3%
	266	239	89.9%	200	83.6%	75.2%
max.	332	303	91.2%	255	84.2%	76.7%

The class-E amplifier has a maximum efficiency of 84.2%, which sums up to a total maximum efficiency of 76.7% for an active power value of $P_L = 255\,\mathrm{W}$ at the reactor coils.

This means that a good efficiency can be realized despite the fact that the system is very loosely coupled, which lies in its nature. Only a higher density of WLEs, i.e., number of WLEs per volume, would increase the coupling, but the WLE density and the desirable light intensity for algae is limited. As stated in [24], higher light intensity leads to photoinhibition and, therefore, reduces bio-efficiency. The strength of the coupling can be quantified by calculating the power factor for the series connection of R and L in the simplified circuit in Figure 5. With the active power $P_L = 255\,\mathrm{W}$ and the current RMS value $I_{RMS} = 3.75\,\mathrm{A}$ (Figure 12), the equivalent resistance

$$R = \frac{P_L}{I_{RMS}^2} \tag{20}$$

is found to be 18.2 Ω. The coil impedance is calculated by

$$X_L = 2\pi f L \tag{21}$$

and found to by 382 Ω. Therefore, the power factor

$$\cos\varphi = \frac{R}{\sqrt{R^2 + X_L^2}} \tag{22}$$

is as low as 0.048.

A comparison of the bio-efficiency of internal and external illumination is given in Figure 13. It shows bio dry weight *BDW* vs. cultivation time for two internally and three externally illuminated cultures. The bio dry weight is determined by washing and filtering part of the culture. The expended electric power has been kept constant for both illumination types in order to guarantee comparability. For the smallest reactor diameter 50 mm, the external illumination gives slightly better results. The reason is that the Lambert-Beer damping is not yet significant at such small diameter and that we have some electrical losses regarding the wireless power transfer. At a diameter of 150 mm, the internal illumination is already superior. Even for the 300 mm diameter reactor, the growth rate stays constant using internal illumination. This proves that the system is suitable for scale-up. An experiment in the 300 mm reactor with external illumination has been omitted, because the expected growth rate would be very small.

Another topic that has to be taken into account is the impact of intermediate frequency electromagnetic fields (IF-EMF) on organisms [33]. It is also important to note that if our bioreactor is operated unshielded, the stray field is within health and safety limitations [34]. Nevertheless, magnetic shielding might be a future issue [35]. The influence of static fields on algae and other microorganisms has already been studied [36,37]. The influence of IF-EMF on algae growth is less understood, but there are no hints of any negative impact [38].

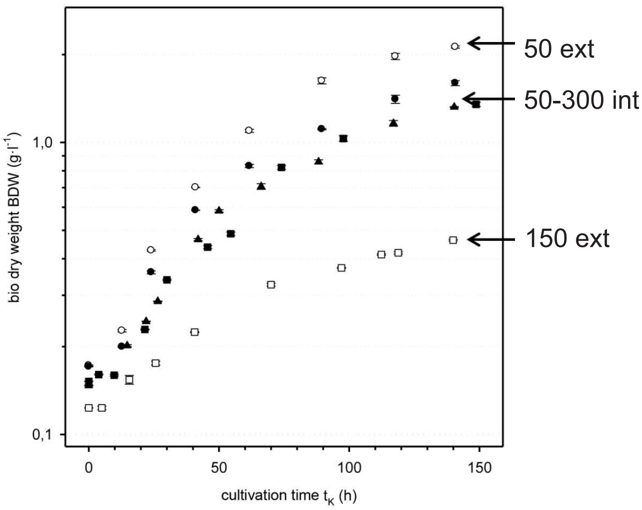

Figure 13. Comparison of internal (int) and external (ext) illumination. The numbers on the right are the diameters of the utilized reactors in mm.

A comparison of our amplifier-reactor combination with other systems is hardly possible, as it is difficult to find similar problems in literature (very loose coupling, numerous receivers). The authors of [11], for example, report about efficiencies of their electric vehicle charging system including a class-E amplifier of up to 88.4%. However, they also proved that small variations of parameters like air gap or vehicle position have great influence on efficiency.

7. Conclusions

This paper discusses a novel concept for the internal illumination of photobioreactors. The novel internal illumination concept showed cultivation results for microalgae *C. reinhardtii* that clearly prove it to be superior to classical external illumination. By comparing bio dry weights of externally and internally illuminated reactor, the suitability of our system for scale-up could be proved. It could further be shown that the class-E amplifier concept suits well for a system with such a high degree of reactive power. In spite of the high amount of reactive power, large efficiency could be reached.

The aim of the novel internal illumination concept is to utilize standard reactor types as photobioreactors. Therefore, the field coil optimization method will have to be extended. Even reactors containing electrically conductive materials are an option. Consequently, further tasks which have to be investigated are field coils for different reactor geometries, and the use of ferrites for shielding. The position of shielding material can also be incorporated into the optimization process. Another challenge is the design and construction of 3D coils for the generation of rotating field vectors.

Author Contributions: A.S. designed, simulated and manufactured the electronic circuits and experiment and wrote the original draft. M.H. designed and conducted the algae cultivation, mainly wrote Section 2 and proofread the manuscript. R.B. did the original conceptualization, design of biotechnological experiments, supervision, writing—review and editing.

Funding: The authors are grateful that this work was financially supported by the German Research Foundation (DFG-GZ: SU 504/2-1 & BU 461/35-1) and that the executing scientist was supported by a scholarship from the 'Deutsche Telekom Stiftung'.

Conflicts of Interest: The authors declare no conflict of interest.

References

1. Si, P.; Hu, A.; Malpas, S.; Budgett, D. A frequency control method for regulating wireless power to implantable devices. *IEEE Trans. Biomed. Circ. Syst.* **2008**, *2*, 22–29. [CrossRef]
2. Friedmann, J.; Groedl, F.; Kennel, R. A novel universal control scheme for transcutaneous energy transfer (TET) applications. *IEEE J. Emerg. Sel. Top. Power Electron.* **2015**, *3*, 296–305. [CrossRef]

3. Hwang, S.H.; Kang, C.G.; Son, Y.H.; Jang, B.J. Software-based wireless power transfer platform for various power control experiments. *Energies* **2015**, *8*, 7677–7689. [CrossRef]
4. Narayanamoorthi, R.; Vimala Juliet, A.; Chokkalingam, B.; Padmanaban, S.; Leonowicz, Z.M. Class E power amplifier design and optimization for the capacitive coupled wireless power transfer system in biomedical implants. *Energies* **2017**, *10*, 1–20.
5. Dai, W.; Tang, W.; Cai, C.; Deng, L.; Zhang, X. Wireless power charger based on class E amplifier with the maximum power point load consideration. *Energies* **2018**, *11*, 2378. [CrossRef]
6. Zeng, F.G.; Rebscher, S.; Harrison, W.; Sun, X.; Feng, H. Cochlear implants: System design, integration, and evaluation. *IEEE Rev. Biomed. Eng.* **2008**, *1*, 115–142. [CrossRef] [PubMed]
7. Carta, R.; Tortora, G.; Thoné, J.; Lenaerts, B.; Valdastri, P.; Menciassi, A.; Dario, P.; Puers, R. Wireless powering for a self-propelled and steerable endoscopic capsule for stomach inspection. *Biosens. Bioelectron.* **2009**, *25*, 845–851. [CrossRef] [PubMed]
8. Carta, R.; Sfakiotakis, M.; Pateromichelakis, N.; Thonè, J.; Tsakiris, D.; Puers, R. A multi-coil inductive powering system for an endoscopic capsule with vibratory actuation. *Sens. Actuators A Phys.* **2011**, *172*, 253–258. [CrossRef]
9. Harrison, R. Designing efficient inductive power links for implantable devices. In Proceedings of the ISCAS 2007, IEEE International Symposium on Circuits and Systems, New Orleans, LA, USA, 20–27 May 2007; pp. 2080–2083. [CrossRef]
10. Zheng, C.; Lai, J.S.; Chen, R.; Faraci, W.; Ullah Zahid, Z.; Gu, B.; Zhang, L.; Lisi, G.; Anderson, D. High-efficiency contactless power transfer system for electric vehicle battery charging application. *IEEE J. Emerg. Sel. Top. Power Electron.* **2015**, *3*, 65–74. [CrossRef]
11. Villa, J.L.; Sallán, J.; Llombart, A.; Sanz, J.F. Design of a high frequency inductively coupled power transfer system for electric vehicle battery charge. *Appl. Energy* **2009**, *86*, 355–363. [CrossRef]
12. Chen, Z.; Wu, Q.; Yuan, Y. A novel zero-voltage-switching push-pull high-frequency-link single-phase inverter. *IEEE J. Emerg. Sel. Top. Power Electron.* **2016**, *4*, 421–434. [CrossRef]
13. Chen, Y.; Xu, D.; Xi, J. Common-mode filter design for a transformerless ZVS full-bridge inverter. *IEEE J. Emerg. Sel. Top. Power Electron.* **2016**, *4*, 405–413. [CrossRef]
14. Sokal, N.; Sokal, A. Class E-A new class of high-efficiency tuned single-ended switching power amplifiers. *IEEE J. Solid-State Circ.* **1975**, *10*, 168–176. [CrossRef]
15. Kazimierczuk, M.; Puczko, K. Exact analysis of class E tuned power amplifier at any Q and switch duty cycle. *IEEE Trans. Circ. Syst.* **1987**, *34*, 149–159. [CrossRef]
16. Choi, U.G.; Yang, J.R. A 120 W class-E power module with an adaptive power combiner for a 6.78 MHz wireless power transfer system. *Energies* **2018**, *11*, 2083. [CrossRef]
17. Barton, T.; Gordonson, J.; Perreault, D. Transmission line resistance compression networks and applications to wireless power transfer. *IEEE J. Emerg. Sel. Top. Power Electron.* **2015**, *3*, 252–260. [CrossRef]
18. Taghavi, H.; Hkansson, B.; Reinfeldt, S. Analysis and design of RF power and data link using amplitude modulation of class-E for a novel bone conduction implant. *IEEE Trans. Biomed. Eng.* **2012**, *59*, 3050–3059. [CrossRef]
19. Wang, G.; Liu, W.; Sivaprakasam, M.; Kendir, G. Design and analysis of an adaptive transcutaneous power telemetry for biomedical implants. *IEEE Trans. Circ. Syst. I Regul. Pap.* **2005**, *52*, 2109–2117. [CrossRef]
20. Jalbrzykowski, S.; Bogdan, A.; Citko, T. A dual full-bridge resonant class-E bidirectional DC-DC converter. *IEEE Trans. Ind. Electron.* **2011**, *58*, 3879–3883. [CrossRef]
21. Heining, M.; Sutor, A.; Stute, S.; Lindenberger, C.; Buchholz, R. Internal illumination of photobioreactors via wireless light emitters: A proof of concept. *J. Appl. Phycol.* **2015**, *27*, 59–66. [CrossRef]
22. Burek, B.O.; Sutor, A.; Bahnemann, D.W.; Bloh, J.Z. Completely integrated wirelessly-powered photocatalyst-coated spheres as a novel means to perform heterogeneous photocatalytic reactions. *Catal. Sci. Technol.* **2017**, *7*, 4977–4983. [CrossRef]
23. Sutor, A.; Heining, M.; Lindenberger, C.; Buchholz, R. A method for optimizing the field coils of internally illuminated photobioreactors. *IEEE Trans. Magn.* **2014**, *50*, 1–4. [CrossRef]
24. Heining, M.; Buchholz, R. Photobioreactors with internal illumination—A survey and comparison. *Biotechnol. J.* **2015**, *10*, 1131–1137. [CrossRef]
25. Carvalho, A.P.; Silva, S.O.; Baptista, J.M.; Malcata, F.X. Light requirements in microalgal photobioreactors: An overview of biophotonic aspects. *Appl. Microbiol. Biotechnol.* **2011**, *89*, 1275–1288. [CrossRef] [PubMed]

26. Fiorillo, F. *Characterization and Measurement of Magnetic Materials*; Academic Press: Cambridge, MA, USA, 2004; pp. 25–36.
27. Lee, B.; Ahn, D.; Ghovanloo, M. Three-phase time-multiplexed planar power transmission to distributed implants. *IEEE J. Emerg. Sel. Top. Power Electron.* **2016**, *4*, 263–272. [CrossRef] [PubMed]
28. Jamal, N.; Saat, S.; Shukor, A. A study on performances of different compensation topologies for loosely coupled inductive power transfer system. In Proceedings of the 2013 IEEE International Conference on Control System, Computing and Engineering (ICCSCE), Penang, Malaysia, 29 November–1 December 2013; pp. 173–178. [CrossRef]
29. Kuipers, J.; Bruning, H.; Yntema, D.; Rijnaarts, H. Wirelessly powered ultraviolet light emitting diodes for photocatalytic oxidation. *J. Photochem. Photobiol. A Chem.* **2015**, *299*, 25–30. [CrossRef]
30. Suetsugu, T.; Kazimierczuk, M.K. Off-nominal operation of class-E amplifier at any duty ratio. *IEEE Trans. Circ. Syst. I Regul. Pap.* **2007**, *54*, 1389–1397. [CrossRef]
31. Raab, F. Idealized operation of the class E tuned power amplifier. *IEEE Trans. Circ. Syst.* **1977**, *24*, 725–735. [CrossRef]
32. Kazimierczuk, M.K. *RF Power Amplifiers*; John Wiley & Sons: Hoboken, NJ, USA, 2014.
33. Shigemitsu, T.; Yamazaki, K.; Nakasono, S.; Kakikawa, M. A review of studies of the biological effects of electromagnetic fields in the intermediate frequency range. *IEEJ Trans. Electr. Electr. Eng.* **2007**, *2*, 405–412. [CrossRef]
34. Litvak, E.; Foster, K.; Repacholi, M. Health and safety implications of exposure to electromagnetic fields in the frequency range 300 Hz to 10 MHz. *Bioelectromagnetics* **2002**, *23*, 68–82. [CrossRef]
35. Dick, C.; Polak, C.; Waffenschmidt, E. Proposal of a figure of merit for the characterization of soft-magnetic shielding material used in inductive wireless power transmission systems. *IEEE J. Emerg. Sel. Top. Power Electron.* **2015**, *3*, 272–279. [CrossRef]
36. Wang, H.Y.; Zeng, X.B.; Guo, S.Y.; Li, Z.T. Effects of magnetic field on the antioxidant defense system of recirculation-cultured *Chlorella vulgaris*. *Bioelectromagnetics* **2008**, *29*, 39–46. [CrossRef] [PubMed]
37. Small, D.P.; Hüner, N.P.; Wan, W. Effect of static magnetic fields on the growth, photosynthesis and ultrastructure of *Chlorella kessleri* microalgae. *Bioelectromagnetics* **2012**, *33*, 298–308. [CrossRef] [PubMed]
38. Nakasono, S.; Ikehata, M.; Dateki, M.; Yoshie, S.; Shigemitsu, T.; Negishi, T. Intermediate frequency magnetic fields do not have mutagenic, co-mutagenic or gene conversion potentials in microbial genotoxicity tests. *Mutat. Res. Gen. Toxicol. Environ. Mutagenes* **2008**, *649*, 187–200. [CrossRef]